Journal of Alloys and Compounds 619 (2015) 800–806

Contents lists available at ScienceDirect

Journal of Alloys and Compounds

journal homepage: www.elsevier.com/locate/jalcom

Near-infrared light emission of Er^{3+}-doped zirconium oxide thin films: An optical, structural and XPS study

J.L. Clabel H. [a,*], V.A.G. Rivera [b], M. Siu Li [b], L.A.O. Nunes [b], E.R. Leite [c], W.H. Schreiner [d], E. Marega Jr. [b]

[a] Departamento de Física, UFSCar, Caixa Postal 676, São Carlos 13565-905, SP, Brazil
[b] Instituto de Física de São Carlos, USP, Caixa Postal 369, São Carlos 13560-970, SP, Brazil
[c] Laboratório Interdisciplinar de Eletroquímica e Cerâmicas, UFSCar, Caixa Postal 676, São Carlos 13565-905, SP, Brazil
[d] Departamento de Física, UFPR, Caixa Postal 19044, Curitiba 81531-980, PR, Brazil

ARTICLE INFO

Article history:
Received 18 May 2014
Received in revised form 23 August 2014
Accepted 1 September 2014
Available online 8 September 2014

Keywords:
Zirconium oxide thin films
Photoluminescence
Near-infrared emission light
XPS
Photoluminescence quenching

ABSTRACT

This paper investigates the near-infrared emission and structural properties of Er^{3+}-doped zirconium oxide thin films modified with a fixed content of zinc oxide. The films were obtained by electron beam deposition on Si(100) substrates, followed by a thermal treatment with or without a controlled oxygen flow. The samples were characterized by X-ray diffraction (XRD), X-ray photoelectron spectroscopy (XPS) and energy dispersive X-ray spectroscopy (EDX). Scanning electron microscopy (SEM) was used to evaluate the surface morphology, distributions and size of the grains in the films. The results confirmed significant changes in these films from thermal treatment with or without oxygen flow. Fourier transform infrared spectroscopy (FTIR) was used to analyze the absorption bands of the films. The photoluminescence (PL) measurement and $^4I_{13/2} \rightarrow {}^4I_{15/2}$ lifetime was measured under 980 nm near-infrared excitation. The effects of thermal treatment as well as the concentration of Er_2O_3 on the PL emission intensity and lifetime in the near-infrared region (from the $^4I_{13/2} \rightarrow {}^4I_{15/2}$ radiative transition) were studied. Thermal treatment under a controlled atmosphere increased the PL emission intensity due to a diminution of the residual OH groups, as confirmed by the XPS and analysis and FTIR spectroscopy. The film modified with 3 mol% of Er_2O_3 content annealed in oxygen flow shows an emission intensity of two orders of magnitude greater than the annealed film without oxygen flow at 1550 nm, nevertheless, the bandwidth was practically the same (7.6 nm) in both cases.

Published by Elsevier B.V.

1. Introduction

Zirconium oxide thin films exhibit several valuable characteristics including chemical stability, high thermo-mechanical resistance, low thermal conductivity, and ionic conductivity [1,2]. In optical devices, zirconium oxide films are excellent candidates due to their high refractive index, low optical loss, and high transparency, enabling them to be used in applications such as waveguides, interferometry, and electro-optical devices [3–5]. Furthermore, the low phonon energy of zirconium oxide can increase the probability of transitions in materials doped with rare-earth ions. As a result, there is interest in their use for photonics applications [6].

Trivalent rare-earth ions can be used to stabilize the structure of crystalline zirconium oxide films, as well as to activate luminescence properties in these films [2]. The charge compensation due to substitution of Zr^{4+} by Er^{3+} ions results in oxygen vacancies in the zirconia lattice, which gives rise to the optical properties of Er^{3+}-doped zirconia films [7]. Furthermore, the addition of ZnO (also called of modifier) during formation of structure crystalline can increase or not the optical properties of these thin films. We must say that this effect has not been studied in detail in the literature. Thereby, in present work ZnO was used as a modifier in Er^{3+}-doped zirconium oxide, due large bandgap of ZnO ($E_g \sim 3.3$ eV) that permits simultaneous emissions at several wavelengths in presence of rare-earth ions [8,9].

This paper investigates the structural and optical properties of thin films doped with different Er_2O_3 nominal contents, keeping zinc-modifier content fixed. Under laser excitation at 980 nm, the films modified show significant increases in the emission intensity of the $^4I_{13/2} \rightarrow {}^4I_{15/2}$ radiative transition for the annealed films in oxygen flow, in comparison with the annealed films without oxygen flow. This increase is due to diminution of the residual OH groups within the films, which was confirmed by XPS analysis and FTIR spectroscopy.

* Corresponding author.
E-mail address: jlch@df.ufscar.br (J.L. Clabel H.).

http://dx.doi.org/10.1016/j.jallcom.2014.09.007
0925-8388/Published by Elsevier B.V.

2. Experimental

The thin film target composition was $(90 - x)ZrO_2 + 10ZnO + xEr_2O_3$ (mol%), where $x = 1$, 2 and 3 mol%, as detailed in Table 1. Besides, were prepared two samples without ZnO (labeled E2), in order to evaluate the ZnO presence in our samples. All the samples were prepared as solid solutions from high purity (>98%) starting materials. The powder was mixed for two hours in a ball mill containing a suspension of zirconia in isopropyl alcohol, then transferred to a beaker, and dried at 100 °C. The resulting powder was ground for 20 min in distilled water in a mortar (using a ratio of 1 g of powder to 50 μL of water), to facilitate the conformation process. Subsequently, ceramic pellets (8 mm diameter and 1.2 mm thick) were formed by pressing at 140 MPa, followed by preannealed at 900 °C for 4 h. The preannealed processes in ceramic pellets facilitate the doped Erbium effect as well as remove possible organic and volatile impurities [10]. The films were produced in an evaporation chamber with a base pressure of 4×10^{-6} mbar, using an electron beam gun (Telemark-231) operated at 6 kV and a current of 40 mA. Tantalum crucibles were used to support the high temperature during evaporation. The conditions used resulted in the homogeneous deposition of hard transparent films (2.6 ± 0.1 μm thickness) on Si(100) substrates (two for each Er_3O_2 concentration), which was confirmed using an FE-SEM instrument (Supra 35-VP, Carl Zeiss, Germany) operated at 15 kV. The films were then submitted to thermal treatment at 1000 °C for 5 h, either with or without O_2 flow.

The crystallinity and phases present in the thin films were investigated by X-ray diffraction (XRD), using a Rigaku Dmax 2500 PC diffractometer operated with Cu Kα radiation. The 2θ range was from 10° to 75°, with steps of 0.02°. Scanning electron microscopy (SEM) was used to investigate the morphology of the thin films. The morphology and quantitative element analysis of the films were investigated by a SEM-EDX instrument (Model XL-30, Philips, Japan) operated at 25 kV. Analysis of the surface of the low temperature-calcined thin films was performed by X-ray photoelectron spectroscopy (XPS), using an ESCA3000 instrument (VG Microtech) with Al Kα radiation and a base pressure of 3×10^{-10} mbar. The spectra were obtained at a take-off angle of 45° to the sample, using a 250 mm hemispherical energy analyzer with an overall energy resolution of 0.8 eV. The elemental quantifications were obtained using the spectrometer software. Standard Shirley background subtraction was employed, and the C 1s peak at 284.5 eV was used for the binding energy calibration. In order to determine the binding energies of the component present in our thin films analysis of the spectra was performed by a fitting procedure using Gaussian peak shapes, Fig. 3.

In order to investigate the OH, Si—O, and Zn—O absorption bands, infrared (IR) measurements were performed in a Fourier transform infrared (FTIR) spectrometer the Perkin Elmer in the range 2250–24,000 nm in our samples. The FTIR spectra data (2250–24,000 nm) of the thin films annealed with and without a flux of O_2 was cut to two different spectral ranges: (i) at the range of 2250–7500 nm and (ii) at the range of 7500–24,000 nm, shown in Fig. 4(a)–(b), respectively.

The measurements of PL were performed using a Thermo Jarrel-Ash Monospec 27 monochromator and a Hamamatsu R446 photomultiplier, with a data acquisition system controlled by a microcomputer. The excitation source was a 980 nm laser diode with 500 mW. The laser beam was focused under grazing incidence on the surface of the film, which was placed in front of the monochromator slit where the film emission was collected through a convergent lens. For measuring the $^4I_{13/2} \rightarrow {}^4I_{15/2}$ lifetime, the samples were irradiated with the laser diode using a pulse width of 100 ns. The lifetime was calculated using the expression $I(t) = I_0 \exp[-t/\tau]$, where I_0 is the intensity at time zero. The emission signal was recorded on an oscilloscope. Multiple PL measurements were made in order to provide confidence in the reproducibility of the procedure when the sample was moved in the laser beam or removed and replaced in the apparatus. The laser beam was always focused on the center of the film, with fixed incidence and collection angles of 10°.

3. Results and discussion

The crystallinity of the thin films, according to the Er_2O_3 content, is shown in Fig. 1(a)–(b) for annealing without and with O_2 flow, respectively. All the peaks of Fig. 1(a) were indexed as a cubic phase with the Fm-3m space group identified with **c** letter, which

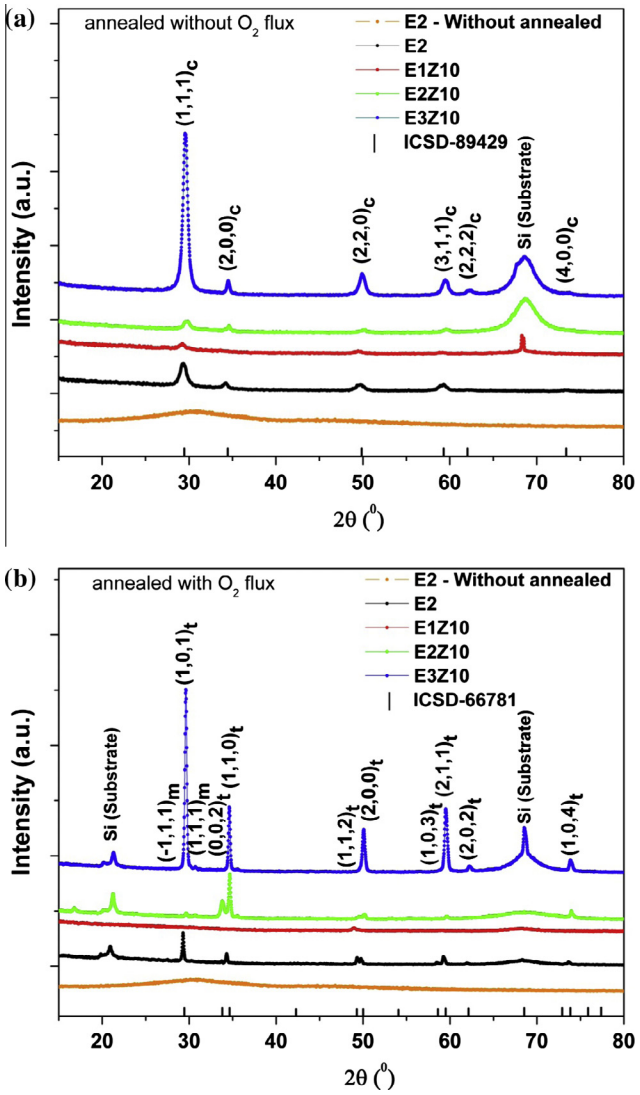

Fig. 1. XRD spectra of the samples annealed at 1000 °C for 5 h, (a) without O_2 flow, and (b) with O_2 flow. The cubic phase peaks are indicated with the letters **t** (tetragonal phase) and **m** (monoclinic phase).

is in agreement with the Inorganic Crystal Structure Database (ICSD) entries No. 89429 [11], while the diffractograms of Fig. 1(b) corresponded to a tetragonal phase with the P42/nmcz space group identified with **t** letter, with ICSD No. 66781 [12]. Also, it is observed from Fig. 1(b), for E3Z10 sample, subtle peaks corresponding to the monoclinic phase identified with **m** letter, ICSD No. 18190 [13]. The Er_2O_3 content was a determining factor in the structure and crystal formation of these thin films. The degree of crystallinity was influenced by three factors: (i) deposition technique, (ii) content of Er_2O_3 and (iii) the annealing procedure (with or without a flow of O_2).

Table 1
Labeling, target composition, and atomic percentage of the erbium ions in the thin films.

Label	Composition (mol%)	Average size-grain (nm)		Content (at.%) of erbium	
		Without O_2	With O_2	Without O_2	With O_2
E2	$98ZrO_2$–$2Er_2O_3$	50	100	1.49	1.90
E1Z10	$89ZrO_2$–$10ZnO$–$1Er_2O_3$	35	190	0.12	0.19
E2Z10	$88ZrO_2$–$10ZnO$–$2Er_2O_3$	40	200	0.69	0.70
E3Z10	$87ZrO_2$–$10ZnO$–$3Er_2O_3$	60	125	1.57	1.65

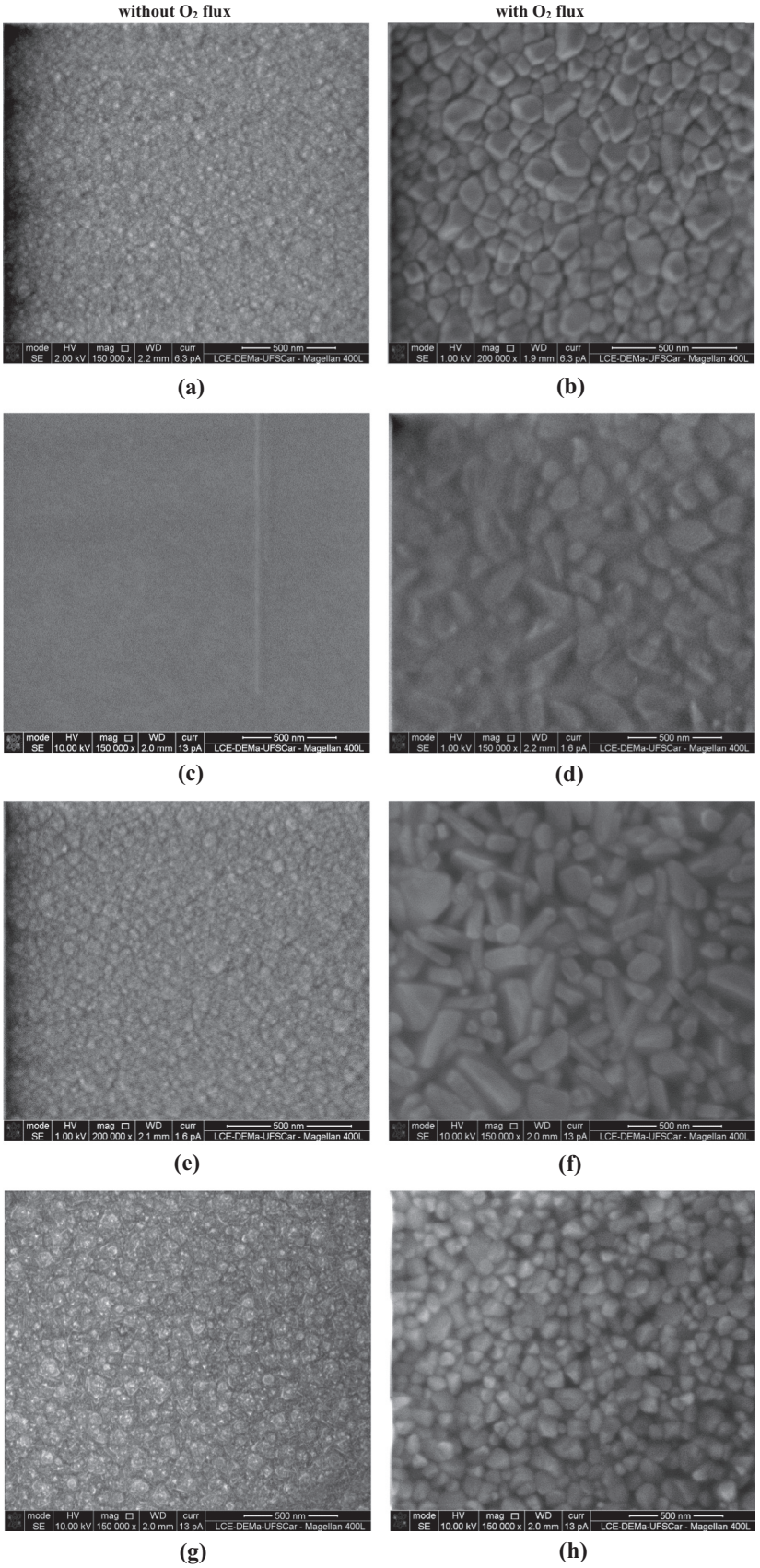

Fig. 2. Surface morphology of the films annealed without O_2 flow for (a) E2, (c) E1Z10, (e) E2Z10 and (g) E3Z10 and (b), thin films annealed with O_2 flow for (b) E2, (d) E1Z10, (f) E2Z10 and (h) E3Z10.

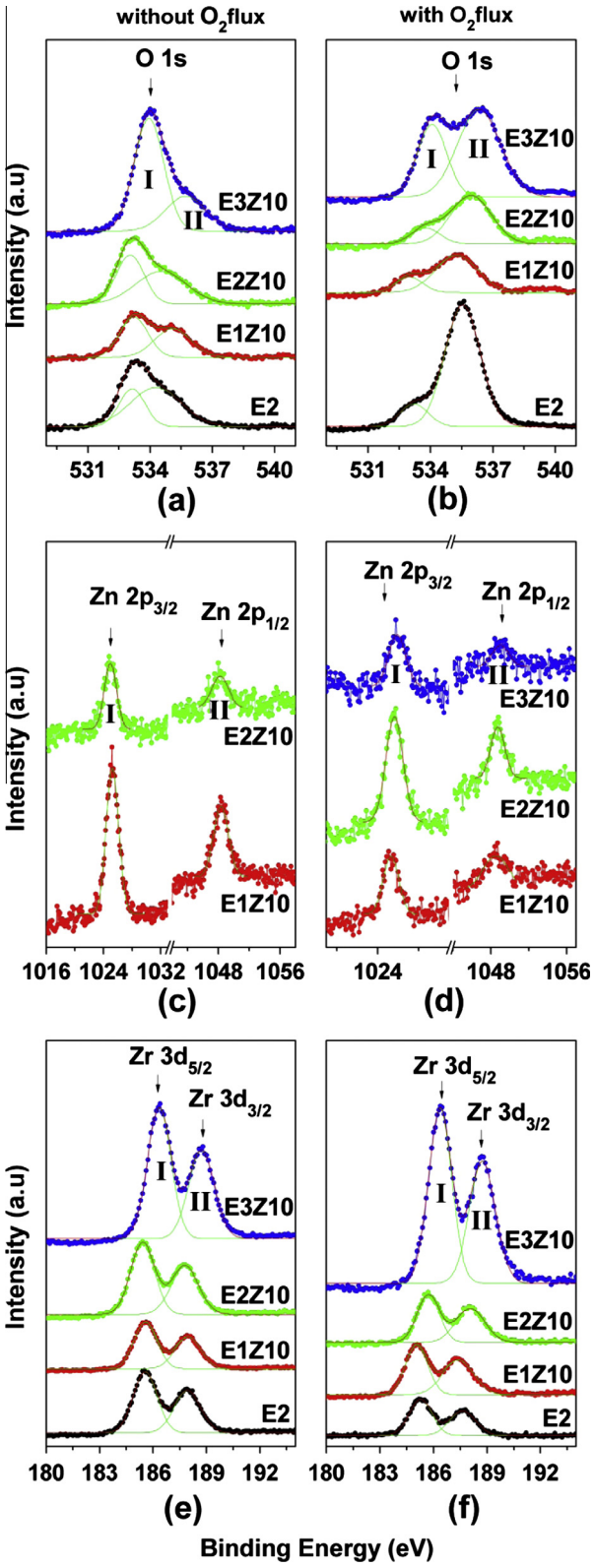

Fig. 3. Curve fitting results for the binding energy spectra of thin films annealed without O_2 flow for (a) O 1s, (c) Zn 2p, and (e) Zr 3d, and thin films annealed with O_2 flow for (b) O 1s, (d) Zn 2p, and (f) Zr 3d.

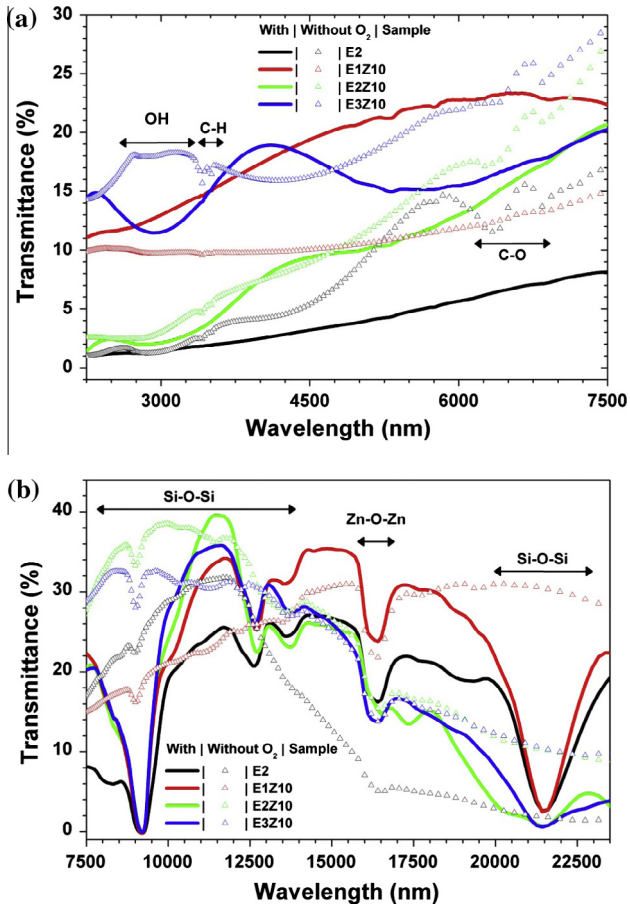

Fig. 4. FTIR analyses of the thin film annealed with (left) and without (right) O_2 flow at 1000 °C/4 h.

Previous XRD measurements of Er_2O_3-doped ZrO_2 thin films demonstrated the crystalline nature of films deposited by the EB-PVD process onto quartz (100) substrates, submitted to evaporation at room temperature, and heating at 426 °C [7,10]. Cabello et al. [14], showed the non-crystalline characteristics of thin films formed on a Si(100) substrate by a photodeposition process at room temperature, followed by an annealing treatment under a continuous flow of synthetic air at 500 °C for 2 h. On the other hand, crystalline thin films were produced by spin-coating onto quartz substrates at room temperature, followed by annealed at 1000 °C for 6 h [15]. Therefore, the crystallinity of the film is influenced also by the deposition technique, Er_2O_3 content, as well as, annealing treatment with or without flow of O_2. The thin films under thermal treatments without (with) O_2 flow, resulted in films with a low (high) degree of crystallinity, growth along the preferred direction (111) or (101) for phases cubic and tetragonal, respectively, Fig. 1(a)–(b). Furthermore, although the introduction of oxygen should considerably reduce preferential growth along the (101) direction, due to contamination of the grain boundaries of the growing films by the segregated oxygen atoms [16–18], this did not occur in the present case, Fig. 2.

Despite that the pure zirconia has a monoclinic structure up to a temperature of 1100 °C, there is changes to the tetragonal phase in the range 1100–2370 °C. For temperatures higher than 2370 °C zirconia adopts a cubic phase [19]. In pure zirconia the presence of oxygen vacancies was found as a key factor to the stabilization of high temperature ZrO_2 polymorphs [20]. In this manner, oxygen vacancies can be introduced into the ZrO_2 lattice during the process of thermal treatments resulting in the **t**-ZrO_2 stabilization. Therefore, the incorporation of O_2 flow in the annealed process strongly interacts with the zirconia surface sites and a **t**-ZrO_2 → **m**-ZrO_2 transition is more possible. Then, the presence of O_2 flow can cause the appearance of both **t**-ZrO_2 and **m**-ZrO_2 phases, Fig. 1(b).

EDX analysis revealed an increase of the atomic percentage of the erbium ions in all the samples when increasing the nominal content of Er_2O_3 for the thin films modified with zinc oxide. However, such values are lower in comparison with the not modified films, E2Z10 and E2, Table 1. Besides, a subtle increase of the atomic percentage of the erbium ions is observed in the films modified under O_2 flow in comparison with the films without O_2 flow.

The morphology of the surfaces of thin films annealed without and with O_2 flux is shown in Fig. 2. The entire SEM images clearly show the average size of the grains is of the order of nanometer, being higher in thin films with O_2 flux, see Table 1. The thin film without O_2 flux observed in the Fig. 2, shows what the size grains are uniformly distributed over the surface and good connectivity between the grains. In this sense, the size grains increases slightly with increasing of Er_2O_3 content, nevertheless, for the E2 and E2Z10 samples (without O_2 flow) keeping fixed the Er_2O_3 content a decrease grain size is observed, Table 1, which is assigned to the ZnO modifier presence. On the other hand, in O_2 flow is possible to observe grains sizes are uniformly distributed over the surface, Fig. 2. With increase of Er_2O_3 content for E1Z10 and E2Z10, causes more defects greatly degenerate the grains size and shape leading to pores and less compact thin films, suggesting a deterioration of the crystallinity, Fig. 1(b). However, E3Z10 is observed grains size homogeneous, uniformly distributed over the surface with high crystallinity. Besides, for the E2 and E2Z10 samples (with O_2 flow) an increase in the size and shape of the grain is observed, Table 1. In both cases (with or without O_2 flow), we can say that microstructural properties is influenced by the presence of ZnO as well as in low Er_2O_3 content (1% and 2%) with a ZnO fixed content, leading to the presence of pores. The presence of pores directly affects the optical properties, since pore size and distribution can significantly contribute to increasing optical losses due to scattered light in the inter-grain region. This result agrees well with the XRD analysis mentioned above.

A typical XPS spectrum of the thin films is shown in Fig. 3. The binding energies of the core level peaks and the surface compositions are summarized in Table 2.

3.1. O 1s peaks

Fig. 3(a)–(b) shows the O 1s XPS spectra for the thin films annealed with and without a flow of O_2, using different concentrations of Er_2O_3. For both annealing conditions, the surface O 1s peaks were fitted by two nearly Gaussian curves (detailed in Table 2). For thin films annealed without a flow of O_2, the high binding energy components located at 535.1 eV (II) and 535.7 eV (II) could be attributed to the presence of O^{2-} ions due to the oxygen-deficient regions of the subsurface within the ZrO_2 matrix [21]. The lower energy regions located at 533–534 eV (I) and 534.2–534.6 eV (II) (Fig. 3(a)) were related to the O^{2-} ions on the Zr^{4+} structure. The peak intensity was determined by variations in the O—Zr/O—Er/O—Zn binding, as well as the OH bond, confirmed IR measurement, Fig. 4(a).

The analysis of the binding energy for the material prepared under an O_2 flow is shown in Fig. 3(b). Here, peak II was more significant than peak I, in contrast to the thin films annealed without O_2. The higher energy peaks located at 535.5 eV (II) and 536.5 eV (II) corresponded to chemisorbed or OH-bonded water molecules on the surface [22]. The medium binding energy peaks located at 535.2 eV (I) and 535.9 eV (II) were associated with O^{2-} ions in the oxygen-deficient regions within the ZrO_2 matrix [21] indicating that Er_2O_3 and ZnO improved the stability of these thin films. The low binding energy components in Fig. 3(b), located at 533.2 eV (I), 533.6 eV (I), 533.0 eV (I), and 534.1 eV (I) were attributed to O^{2-} ions on the Zr^{4+} structure, which increment with the increase of the Er_2O_3 content.

3.2. Zn 2p peaks

For each element, the Zn 2p binding energy and shape show little change for films with different Er_2O_3 concentration annealed with and without a flow of O_2. Fig. 3(c)–(d) shows the doublet spectral lines of Zn 2p at binding energies of 1022.3–1025.8 eV (Zn $2p_{3/2}$) and 1047.8–1049 eV (Zn $2p_{1/2}$). The energy difference between $2p_{1/2}$ and $2p_{3/2}$ was 23.2 eV, in agreement with the results for Zn^{2+} in Refs. [23,24].

3.3. Zr 3d peaks

Fig. 3(e)–(f) presents the spectra for Zr 3d. For the thin film annealed without O_2 (Fig. 3(e)), the low binding energy peaks located at 185.4 eV (I), 185.6 eV (I), 185.5 eV (I), and 186.4 eV (I) could be attributed to the peaks of Zr^{4+} ions in ZrO_2 [25]. The highest binding energy peaks corresponding to Zr $3d_{5/2}$ were located at approximately 187.9 eV (II), 187.8 eV (II), 187.9 eV (II), and 188.7 eV (II). However, the E2 and E2Z10 samples showed a slight increase of energy with the increase of the Er_2O_3 content, Table 2. For the thin films annealed with O_2, the binding energy of peaks I and II showed only a slight shift with respect to the thin films annealed without O_2. The broader $3d_{5/2}$ and $3d_{3/2}$ peaks for I and II could be explained by the polycrystalline nature of the ZrO_2 phase of this matrix for the thin films annealed without (left) and with O_2 (right) flow.

The infrared spectra of the thin films annealed with and without a flux of O_2 are shown in Fig. 4. The spectra reveal that all these film contain a characteristic broad band at 2900 nm due to the OH stretching vibration and small CH and CH_2 band at 3420 nm and 3503 nm vibrations, respectively [26], Fig. 4(a). For thin films

Table 2
XPS binding energies of the thin films.

Binding energy (eV)									
Film	Peaks	Annealed without an O_2 flow				Annealed with an O_2 flow			
		O 1s	Zn 2p	Zr 3d	Er 4d	O 1s	Zn 2p	Zr 3d	Er 4d
E2	(I)	533.1	–	185.5	168.2[a]	533.2	–	185.2	170.7[a]
	(II)	534.2	–	187.9	–	535.5	–	187.6	–
E1Z10	(I)	533.2	1025.2	185.5	–	533	1025.8	185.1	–
	(II)	535.1	1048	187.9	–	535.2	1048.6	187.4	–
E2Z10	(I)	533	1025.2	185.6	167.1[a]	533.6	1025.6	185.7	168.2[a]
	(II)	534.6	1048.2	187.8	–	535.9	1048.7	188	–
E3Z10	(I)	534	1022.3[a]	186.4	168.6[a]	534.1	1025.8	186.4	166.6[a]
	(II)	535.7	1047.8[a]	188.7	–	536.5	1049.0	188.7	–

[a] Values obtained from a survey of XPS spectra.

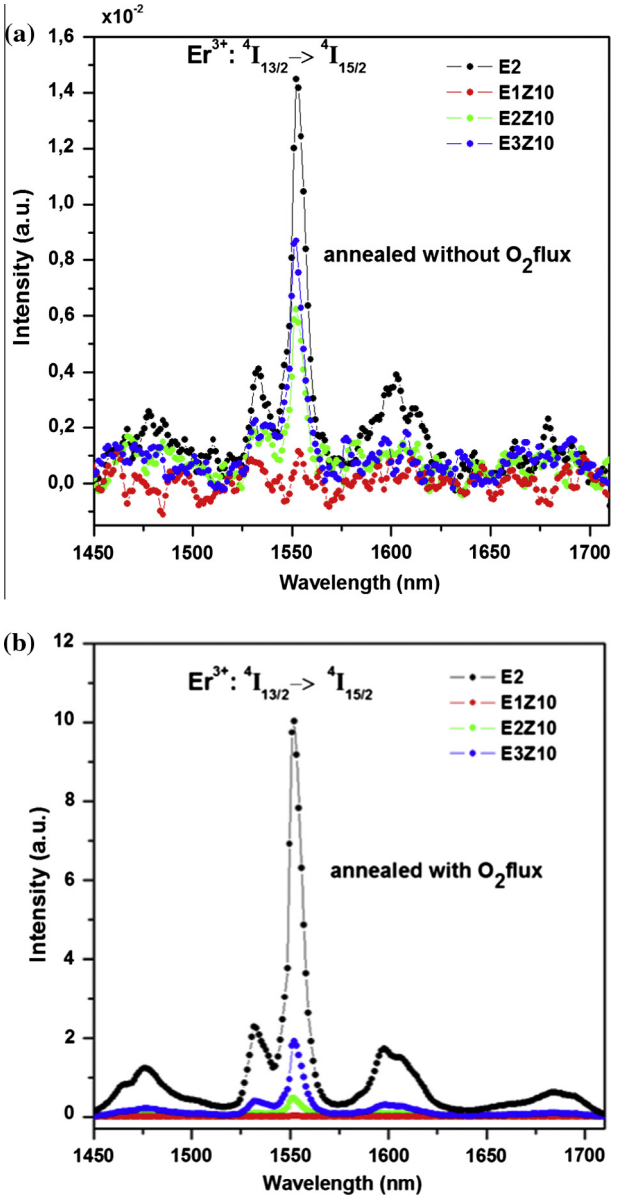

Fig. 5. Near-infrared photoluminescence spectra of thin films prepared on a Si(100) substrate and annealed (a) without O_2 flow, and (b) with O_2 flow.

annealed without O_2 flow the bands intensities of CH and CH_2 increase with increasing Er_2O_3 concentration, however these bands disappear for thin films annealed with O_2 flow, suggesting that dehydrogenation occurs. On the other hand, the bands intensities OH decrease with the increase of the Er_2O_3 concentration in both cases (with and without O_2 flow). The band intensities are slightly higher in thin film annealed without O_2 flow. These bands intensities indicate that the OH groups are distributed on the pore surface [27]. This is in agreement with the micrographs of thin films annealed at O_2 flow, because the porosity decreases with the increasing of the Er_2O_3 content, Fig. 2. Thin films annealed without O_2 flow the band appearing at 6339 nm and 6840 nm correspond to C═O stretching [28]. The strong band at 9193 nm, 12,650 nm and 21,520 nm (with O_2 flow) in all the spectra are attributed to the Si—O—Si stretching (asymmetric), rocking and bending vibrations indicate the formation of the SiO_2 network [26,27,29], has diminished notably in 9193 nm and practically disappeared in 12,650 nm and 21,520 nm for thin films annealed without O_2 flow. The band observed at 16,103 nm is assigned to the Zn—O—Zn

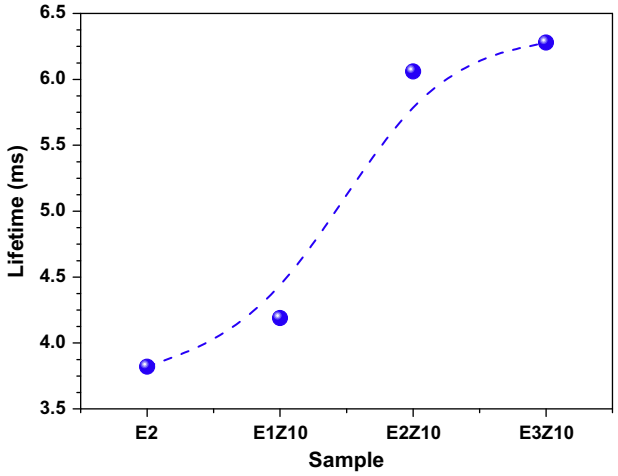

Fig. 6. Lifetime of the $^4I_{13/2}$ level as a function of erbium content. The dotted line is a guide for the eyes. Samples with O_2 flow.

stretching vibrations for all thin films and are corroborated by available literature data [30]. This is probably due to a substitution of Zn^{2+} ions by Zr^{4+} ions in the crystal lattice structure.

So for, both characterization XPS and infrared spectra shown a decrease of the OH contained with the increasing Er_2O_3 concentration, and XRD shown an increase of the crystallinity with the increase of the Er_2O_3 concentrations, i.e. we are stabilizing the crystalline structure of our thin films with increasing Er_2O_3 concentration which is favored by the addition of ZnO and thermal treatments with or without O_2 flow.

The PL spectra are shown in Fig. 5. The peak emission intensity increased with increasing Er^{3+} for the films annealed without O_2 flow (Fig. 5(a)). However, for the thin films annealed with O_2 flow (Fig. 5(b)), the Er^{3+} emission intensities also increased with the concentration of Er^{3+}, by up to two orders of magnitude, reaching a maximum value at 3 mol% Er_2O_3. This could have been due to energy transfer from the host to the loaded ion, and to increased interaction between Er^{3+} ions and available oxygen in the matrix. The PL properties depend on the lengths of bonds between the dopant metal and the oxygen in the matrix [31]. The intensity variation suggested that Er^{3+} was distributed either in the interior or far from residual OH groups (which could cause PL quenching) at the surface of ZrO_2 [32]. In addition, the optimization of Er^{3+} PL in these samples could be explained by a reduction in the OH content such as was verified in Figs. 3 and 4, due to formation of ZrO_2, as well as the increase Er^{3+} content in the thin films modified, Table 1. The emission peak due to the $^4I_{13/2} \rightarrow {}^4I_{15/2}$ transition of the Er^{3+} ion was observed at 1550 nm, with a bandwidth short of 6.8–7.6 nm, which increased with the Er^{3+} content under both conditions. This bandwidth emission should be very useful for applications involving broadband erbium-doped solid lasers, even though the measured FWHM was much lower than that shown by erbium-doped glass ($\geqslant$60 nm) [33,34].

The slight shift of the FWHM center from 1552.3 to 1552.7 nm for thin films annealed with and without a flow of O_2 was due to the effect of splitting of degenerate energy levels in the crystalline phase [10,35].

Lifetime measurements are presented in Fig. 6 as a function of Er_2O_3 content for the samples prepared with O_2 flow during the thermal treatment, since this procedure resulted in a large increase in the emission intensity (Fig. 5). The measurements were performed with a 10 nm bandwidth filter centered at 1552 ± 2 nm, and revealed the dependence on the erbium content (Fig. 6). The quenching effect of concentration on the lifetime was not considered [36], despite the reductions in the emission intensity (Fig. 5)

and the increase in the excited-state lifetime with the erbium content for the samples with ZnO. We assign such results to the cross-relaxation effects between the Er^{3+} ions, owing the increase the Er^{3+} concentration within the films, verified through the EDX analysis. The lifetime behavior of the Er^{3+} centers followed a single-exponential decay, indicating that the $^4I_{13/2}$ level presented one type of emission center, despite the heterogeneous distribution of these emission centers (Fig. 6) [36].

As a final point, the findings of this work demonstrate that Er^{3+}-doped zirconium oxide thin films fabricated without ZnO modification exhibit high PL intensities and short bandwidths, making them very attractive for waveguide with short bandwidth laser and as substrate to fabrication of nanoplasmonic devices [35–37].

4. Conclusions

Zirconium oxide thin films doped with Er^{3+} and modified with zinc oxide were prepared by electron beam evaporation and annealing with and without O_2 flow. Characterization of the thin films annealed with and without O_2 at 1000 °C revealed a distorted and mixed lattice formed by tetragonal, monoclinic and cubic zirconia. The photoluminescence lifetime and optical properties of the films are dependent on the concentration of the doping agent and the annealing procedure. The emission intensity of the Er^{3+} ions increased when the thin films were annealed under O_2, due to reductions of the residual OH groups responsible for photoluminescence quenching. The reduction of OH groups was confirmed by XPS analysis. For the film annealed without O_2, low photoluminescence intensity for lower dopant concentrations (x = 1 and 2 mol%) suggested the formation of defects due to the high concentration of oxygen vacancies relative to the Er^{3+} ions, contrary to observed when annealed with O_2 flow. The lifetime measurements indicated that the films showed cross-relaxation effects in the presence of ZnO, then; this cross relaxations is responsible by the low emission intensity in thin films with the same Er_2O_3 concentration with and without oxygen flow. Despite that the emission intensity drastically decreased with the presence of zinc oxide in general, this zinc-modifier improves the solubility of the erbium ion into the zirconium oxide films, verified through the EDX analysis. This increase of the erbium ions is responsible by the increase the emission intensity and larger lifetime of Er^{3+} ion in the modified samples. Opening us new opportunities of photonic films with high concentrations of rare-earth and large lifetime which could be used in integrated optics with well-developed silicon technologies.

Acknowledgements

This research was supported by the Brazilian agencies CAPES, FAPESP (Process 2009/08978-4), and INOF/CEPOF (Instituto Nacional de Óptica e Fotônica/Centro de Pesquisa em Óptica e Fotônica, São Paulo, Brazil).

References

[1] K.P.S.S. Hembram, G.M. Rao, Properties of zirconia thin films prepared by reactive magnetron sputtering, Mater. Lett. 61 (2007) 502–505.
[2] M.G. Krishna, K.N. Rao, S. Mohan, Structural and optical properties of zirconia thin films, Thin Solid Films 193 (1990) 690–695.
[3] C. Urlacher, C.M. Lucas, E. Bernestein, B. Jacquier, J. Mugnier, Study of erbium doped ZrO_2 waveguides elaborated by a sol–gel process, Opt. Mater. 12 (1999) 19–25.
[4] N.L. Zhang, Z.T. Song, Q. Wan, Q.W. Shen, C.L. Lin, Interfacial and microstructural properties of zirconium oxide thin films prepared directly on silicon, Appl. Surf. Sci. 202 (2002) 126–130.
[5] C.Y. Ma, F. Lapostolle, P. Briois, Q.Y. Zhang, Effect of O_2 gas partial pressure on structures and dielectric characteristics of rf sputtered ZrO_2 thin films, Appl. Surf. Sci. 253 (2007) 8718–8724.
[6] E. De la Rosa-Cruz, L.A. Díaz-Torres, R.A. Rodríguez-Rojas, M.A. Meneses-Nava, O. Barbosa-García, Luminescence and visible upconversion in nanocrystalline ZrO_2:Er^{3+}, Appl. Phys. Lett. 83 (2003) 4903–4907.
[7] F.S. De Vicente, A.C. De Castro, M.F. De Souza, M. Siu Li, Luminescence and structure of Er^{3+} doped Zirconia films deposited by electron beam evaporation, Thin Solid Films 418 (2002) 222–227.
[8] L. Douglas et al., Influence of doping rate in Er^{3+}:ZnO films on emission characteristics, Opt. Lett. 33 (2008) 815–817.
[9] Y. Terai et al., Structural and luminescent properties of Er-doped ZnO films grown by metalorganic chemical vapor deposition, J. Vac. Sci. Technol., B 27 (2009) 2248.
[10] V.A.G. Rivera, F.A. Ferri, J.L. Clabel H., M.K. Kawamura, M.A. Pereira-da-Silva, L.A.O. Nunes, M. Siu Li, E. Marega Jr., High near-infrared emission intensity of Er^{3+}-doped zirconium oxide films on a Si(100) substrate, Proc. SPIE 8621 (2013). 86211K-1–86211K-9.
[11] D.-N. Wang, Y.-Q. Guo, K.-M. Liang, K. Tao, Crystal structure of zirconia by Rietveld refinement, Sci. China 42 (1999) 80–86.
[12] B.Ya. Bondars, G. Heidemane, J. Grabis, K. Laschke, H. Boysen, J. Schneider, F. Frey, Powder diffraction investigations of plasma sprayed zirconia, J. Mater. Sci. 30 (1995) 1621–1625.
[13] D.K. Smith, W. Newkirk, The crystal structure of Baddeleyite (monoclinic ZrO_2) and its relation to the polymorphism of ZrO_2, Acta Cryst. 18 (1965) 983–991.
[14] G. Cabello, L. Lillo, C. Caro, G.E. Buono-Core, B. Chornik, M.A. Soto, Structure and optical characterization of photochemically prepared ZrO_2 thin films doped with erbium and europium, J. Non-Cryst. Solids 354 (2008) 3919–3928.
[15] L.-J. Lai, T.-C. Chu, M.-I. Lin, Y.-K. Lin, Photoluminescence of thin films ZrO_2:Er^{3+} excited by soft X-ray, Solid State Com. 144 (2007) 181.
[16] G. Štefanic, B. Gržeta, S. Music, Influence of oxygen on the thermal behavior of the ZrO_2–Fe_2O_3 system, Mater. Chem. Phys. 65 (2000) 216–221.
[17] A. Eichler, Tetragonal Y-doped zirconia: structure and ion conductivity, Phys. Rev. B 64 (2001) 174103–174111.
[18] D. Sangalli, A. Lamperti, E. Cianci, R. Ciprian, M. Perego, A. Debernardi, Role of oxygen vacancies on the structure and density of states of iron-doped zirconia, Phys. Rev. B 87 (2013) 085206–085216.
[19] J.C.C. Fan, J.B. Goodenough, X-ray photoemission spectroscopy studies of Sn-doped indium-oxide films, J. Appl. Phys. 48 (1977) 3524–3528.
[20] T.L. Barr, An ESCA study of the termination of the passivation of elemental metals, J. Phys. Chem. 82 (1978) 1801–1810.
[21] X.Q. We, B.Y. Man, M. Liu, C.S. Xue, H.Z. Zhuang, C. Yang, Blue luminescent centers and microstructural evaluation by XPS and Raman in ZnO thin films annealed in vacuum, N_2 and O_2, Phys. B 388 (2007) 145–152.
[22] J.F. Moulder, W.F. Stickle, P.E. Sobol, K.D. Bomben, Handbook of X-ray Photoelectron Spectroscopy, Perkin–Elmer Corporation, Eden Prairie, MN, 1992, pp. 88–89.
[23] J. Zhang, D. Gao, G. Yang, J. Zhang, Z. Shi, Z. Zhang, Z. Zhu, D. Xue, Synthesis and magnetic properties of Zr doped ZnO Nanoparticles, Nanoscale Res. Lett. 6 (2011) 587.
[24] D. Blanc, W. Zhang, C. Massard, J. Mugnier, Synthesis and characterisation of tantalum-incorporating silica hybrid sol–gel thin films for optical applications, Opt. Mater. (Amst.) 28 (2006) 331.
[25] J.L. Ferrari, K.O. Lima, L.J.Q. Maia, R.R. Gonçalves, Sol–gel preparation of near-infrared broadband emitting Er^{3+}-doped SiO_2–Ta_2O_5 nanocomposite films, Thin Solid Films 519 (2010) 1319–1324.
[26] I. Uhlmann, D. Hawelka, E. Hildebrandt, J. Pradella, J. Rödel, Structure and mechanical properties of silica doped zirconia thin films, Thin Solid Films 527 (2013) 200–204.
[27] R.M. Almeida, C.G. Pantano, J. Appl. Phys. 68 (1990) 4225.
[28] Prashant K. Sharma, Avinash C. Pandey, G. Zolnierkiewicz, Nikos Guskos, C. Rudowicz, J. Appl. Phys. 106 (2009) 094314.
[29] L. Chen, Y. Liu, Y. Li, Preparation and characterization of ZrO_2:Eu^{3+} phosphors, J. Alloys Comp. 381 (2004) 266–271.
[30] R. Brenier, J. Mugnier, E. Mirica, XPS study of amorphous zirconium oxide films prepared by sol–gel, Appl. Surf. Sci. 143 (1999) 85–91.
[31] W.J. Miniscalco, Erbium-doped glasses for fiber amplifiers at 1500 nm, J. Lightwave Technol. 9 (1991) 234–250.
[32] Q. Chen, M. Ferraris, D. Milanese, Y. Menke, E. Monchiero, G. Perrone, Novel Er-doped PbO and B_2O_3 based glasses: investigation of quantum efficiency and non-radiative transition probability for 1.5 μm broadband emission fluorescence, J. Non-Cryst. Solids 324 (2003) 12–20.
[33] V.A.G. Rivera, M. El-Amraoui, Y. Ledemi, Y. Messaddeq, E. Marega Jr., Expanding broadband emission in the near-IR via energy transfer between Er^{3+}–Tm^{3+} co-doped tellurite-glasses, J. Lumin. 145 (2014) 787–792.
[34] V.A.G. Rivera, L.C. Barbosa, Spectroscopic properties of Er^{3+}-doped sodium-modified tellurite glasses for use as optical amplifiers at 1540 nm, <http://dx.doi.org/10.1016/j.jlumin.2014.07.023>.
[35] V.A.G. Rivera, F.A. Ferri, S.P.A. Osorio, L.A.O. Nunez, A.R. Zanatta, E. Marega Jr., Luminescence enhancement of Er^{3+} ions from electric multipole nanostructure arrays, Proc. SPIE 8269 (2012). 82692H1–82692H7.
[36] V.A.G. Rivera, F.A. Ferri, J.L. Clabel H., M.A. Pereira-da-Silva, L.A.O. Nunes, M. Siu Li, E. Marega Jr., High red emission intensity of Eu:Y_2O_3 films grown on Si(100)/Si(111) by electron beam evaporation, J. Lumin. 148 (2014) 186–191.
[37] V.A.G. Rivera, F.A. Ferri, S.P.A. Osorio, L.A.O. Nunez, A.R. Zanatta Sr., E. Marega Jr., Focusing surface plasmons on Er^{3+} ions with convex/concave plasmonic lenses, Proc. SPIE 8269 (2012). 82692I1–82692I6.